# Conduit processes at the Haukadalur geyser-hosting hydrothermal field (Iceland) revealed by in-situ temperature and high-speed camera measurements.

**Marine Collignon[1], Laura Pioli[1,2], Daniele Trippanera[3], Aurore Carrier[1,4], and Matteo Lupi[1]**

[1]Department of Earth Sciences, University of Geneva, Switzerland.
[2]Department of Chemical and Geological Sciences, University of Cagliari, Italy.
[3]Department of Earth Sciences and Engineering, King Abdullah University of Science and Technology (KAUST), Saudi Arabia.
[4]ADRGT, Grenoble, France.

**Key Points:**

- In-situ temperature evolution from an active geyser reveals heat transfer from a deep aquifer and a bubble trap.
- Geyser connections suggested by synchronous in-situ temperature measurements.
- Details of a water jet eruption captured by high-speed camera.

Corresponding author: Marine Collignon, Marine.Collignon@unige.ch

## Abstract

Geysers fascinated scientists and visitors for several centuries. However, many driving mechanisms such as heat transfer in the conduit or the interconnection of the plumbing system remain poorly understood. We recorded temperature variations inside the active Strokkur's and nearby quasi-dormant Great Geysir's conduits (Iceland), while visually monitoring Strokkur's eruptions at the vent with a high-speed camera. Frequencies of temperature oscillations inside Strokkur highlight both its eruptive behaviour and the general system dynamics. Hydraulic processes also revealed by temperature signals recorded inside Great Geysir, suggesting a connection of both geysers to the same grouundwater reservoir. Our analysis reveals heat transfer from a deep aquifer and a single bubble trap. We propose a model for vapour slug rise, eruption and conduit refill. Each eruption is marked by an initial pulse of liquid water and vapour, between 5 and 28 m/s, generally followed by a second pulse less than a second later. After the eruption, the conduit is refilled by water falling back from the pulses in the pool and drown in from neighbouring groundwater-saturated geological units. The temperature variation during the cooling phase increases with depth while its duration is reduced. This reflects faster heat transfer in the deeper than shallower part of the conduit. The temperature following an eruption also increases with the eruption order, implying larger heat release by multiple eruptions.



## Plain Language Summary

Geysers are hot springs that erupt intermittently. Although they have been studied for several centuries, many aspects such as heat transfer in the conduit and subsurface or geyser interconnection remain poorly understood. We recorded the temperature evolution inside the active Strokkur and the quasi-dormant Great Geysir geysers, located 100 m apart, in the Haukadalur hydrothermal field (Iceland). Analyses of temperature signals suggest that both geysers are connected to the same aquifer at depth. Comparing the timing of eruptions, visually monitored at Strokkur with its temperature records allowed us to characterize the thermal cycle associated with eruptions. Each eruption is followed by a temperature decay and a subsequent temperature rise to which we refer to as cooling and warming phases. We characterise the duration of these phases and the associated temperature variations, which allows us to highlight a faster heat transfer in the deeper than shallower part of the conduit and larger heat release by multiple eruption. High-speed camera revealed the eruption of a water jet in details. Each jet is marked by a first pulse of liquid water and vapour, emitted between 5 and 28 m/s, which is generally followed by a second pulse, less than a second later. We propose a new and complementary model for vapour slug rise, eruption and conduit refill of Strokkur.


## 1 Introduction

Geysers are hot springs that cyclically discharge steam and liquid water and in minor amounts non-condensable gases (e.g. $CO_2$) in jetting eruptions (D. White, 1967; Hurwitz et al., 2016). Natural geysers are rare geological occurrences. Geysers are clustered across a few hydrothermal fields, mainly in Yellowstone

(USA), Geyser Valley (Russia), and El Tatio (Chile) (Bryan, 1995; Hurwitz & Manga, 2017). Their rarity may be due to the peculiar conditions required for their formation. These are a constant water supply, a heat source converting water into vapour and most importantly a permeable system that allows a stable eruptive cycle (e.g. D. White, 1967; Kieffer, 1989; Ingebritsen & Rojstaczer, 1993, 1996; Kiryukhin et al., 2012). The earliest conceptual models for geyser's plumbing systems were derived mostly from observations of the Great Geysir in Iceland (Mackenzie, 1811; Bunsen, 1847). Temperature measurements in the conduits of various geysers (Rinehart, 1969; Noguchi et al., 1983; Hutchinson et al., 1997; Droznin et al., 1999; Munoz Saez et al., 2015; Munoz-Saez et al., 2015) supported ascent-driven decompression boiling in the conduit as the driving mechanism (Bunsen, 1847). However, further geophysical data and/or direct observations of plumbing systems of eroded geysers revealed the existence of one or several laterally-offset cavities connected to the main conduit (Cros et al., 2011; Belousov et al., 2013; Vandemeulebrouck et al., 2013, 2014; Eibl et al., 2021). These observations revive the model initially proposed by Mackenzie (1811), suggesting that eruptions are driven by steam formation in a subsurface cavity. These cavities, known as *bubble traps* act as a reservoir where steam accumulates and periodically discharges into the conduit (Mackenzie, 1811; Belousov et al., 2013; Vandemeulebrouck et al., 2013; Adelstein et al., 2014; Munoz Saez et al., 2015). Geysers have often been considered as smaller and less complex natural analogues of open-conduit volcanic systems (Kieffer, 1984; Hurwitz & Manga, 2017). Because of their more frequent eruptions with respect to their magmatic counterparts, they have been subjected to statistically robust investigations of eruptive dynamics and possible external forcing (Hurwitz & Manga, 2017). Although several authors thoroughly investigated the eruptive dynamics using laboratory experiments (Anderson et al., 1978; Adelstein et al., 2014; Rudolph & Sohn, 2017; Rudolph et al., 2018; Namiki et al., 2016) and multi-disciplinary field investigations (Vandemeulebrouck et al., 2014; Munoz Saez et al., 2015; Munoz-Saez et al., 2015; Eibl et al., 2021), some aspects of geysering are still poorly understood. While direct exploration provided new insights on the morphology of the main conduit (Belousov et al., 2013; Walter et al., 2020), the general subsurface geometry of these systems are rarely known. Recently, Lupi et al. (2022) investigated the hydrogeological structure of the Haukadalur hydrothermal field, Iceland, and based on geoelectrical surveys have shown the strong control that local tectonics exerts on fluid distribution at depth. Seismic data have been used as a proxy to locate the formation and collapse of the vapour slug, providing basic information on heat transfer in the conduit or in the bubble trap (Kedar et al., 1998; Eibl et al., 2021). However, the role of the bubble trap with respect to the deep aquifer in controlling eruptions remains poorly understood. Our general understanding of heat transfer dynamics and its relevance into conduit processes is still hampered by the limited temperature records of successive eruptive cycles and synchronous temperature measurements of different geysers (e.g. Munoz Saez et al., 2015; Munoz-Saez et al., 2015). To fill this gap, in this study we monitored the activity and conduit temperature evolution of the Strokkur and Great Geysir geysers, hosted in the Haukadalur hydrothermal field, Iceland. We selected this hydrothermal field to investigate heat transfer and geyser interaction because of the frequent eruptions and steady recharge at the Strokkur vent (Eibl et al., 2020).

## 2 The Haukadalur hydrothermal field and its geysers

The Haukadalur hydrothermal field is located at the eastern margin of the western volcanic rift zone in the Southern lowlands of Iceland (Fig. 1) at an altitude of about 100 m a.s.l. The heat fueling hydrothermal circulation is provided by a magmatic system that also fed several eruptions in the Late Pleistocene (Saemundsson, 1979; Torfason, 1999; Jones et al., 2007). The Haukadalur field hosts the Great Geysir and the Strokkur geysers, which are amongst the most visited natural touristic attractions of Iceland. This hydrothermal field also hosts hundreds of thermal springs, distributed over a $\sim$3km$^2$ area and along NE-SW to N-S directions (Pasvanoglu, 1998; Torfason, 1999; Walter et al., 2020; Lupi et al., 2022). Written documentation of Great Geysir's and Strokkur's activity dates back to 1294 and 1789, respectively. Furthermore tephrochronological studies showed that the hydrothermal field is active for at least 8000 years (Torfason, 1985). Throughout its known history, Great Geysir's activity has been rejuvenated by large earthquakes before progressively declining and becoming quiescent (Torfason, 1999; Pálmason, 2002). For almost the entire 20$^{th}$ century (1915-2000), the Great Geysir remained inactive unless eruptions were artificially triggered with soap or by lowering the water table (Pálmason, 2002). Two major earthquakes in June 2000 renewed its activity causing the Great Geysir to erupt quasi-yearly. Strokkur's eruptions are different from those of Great Geysir and are characterised by intermittent jets of water into the air with minor amounts of vapour (Torfason, 1999). Strokkur's activity and behaviour have also changed through time. From historical records, eruptions between 1789 and 1896 often lasted for more than one hour with longer intervals between eruptions (Pálmason, 2002). Strokkur was inactive for years when in 1963 its eruptions were renewed by drilling the natural conduit from $\sim$23 to 40 m depth (Torfason, 1999). This made eruptions to occur every 8-12 min. Since the earthquakes in 2000, eruptions of Strokkur are almost twice more frequent and fairly constant (Eibl et al., 2020; Walter et al., 2020). Based on a one-year seismic catalogue, Eibl et al. (2019) showed that eruptions consist of 1 to 6 explosion sequences and that the mean repose times ('waiting time') after single to sextuple eruptions before the next eruption linearly increases from 3.7 to 16.4 min.

Walter et al. (2020) explored the geometry and average temperature gradient of Great Geysir's and Strokkur's conduits down to 20 m depth. Both conduits in their upper parts ($<$ 9-10 m) are pipe-shaped, with a sub-circular section and narrow down from surface to 5 m depth (Fig. 3). Below 10 m depth the conduits have an elliptical section. The temperature inside the conduits (measured during quiescent periods) remains below the boiling point of pure water down to 10 m depth. (Walter et al., 2020).

## 3 Methods

Between the 20$^{th}$ and 23$^{rd}$ of June 2018, we recorded the temperature inside both Strokkur's and Great Geysir's conduits at different depths during several hours at night. We immersed sensors (Hobo U12-015) in the conduits attached to a weighted metallic cable (Table 1). In absence of pressure loggers, we estimated the depth of the temperature records from the measured cable length below the water table. We considered a conservative uncertainty of about 1 m and 2 m at Strokkur and Great Geysir, respectively. Sensor accuracy ranges from

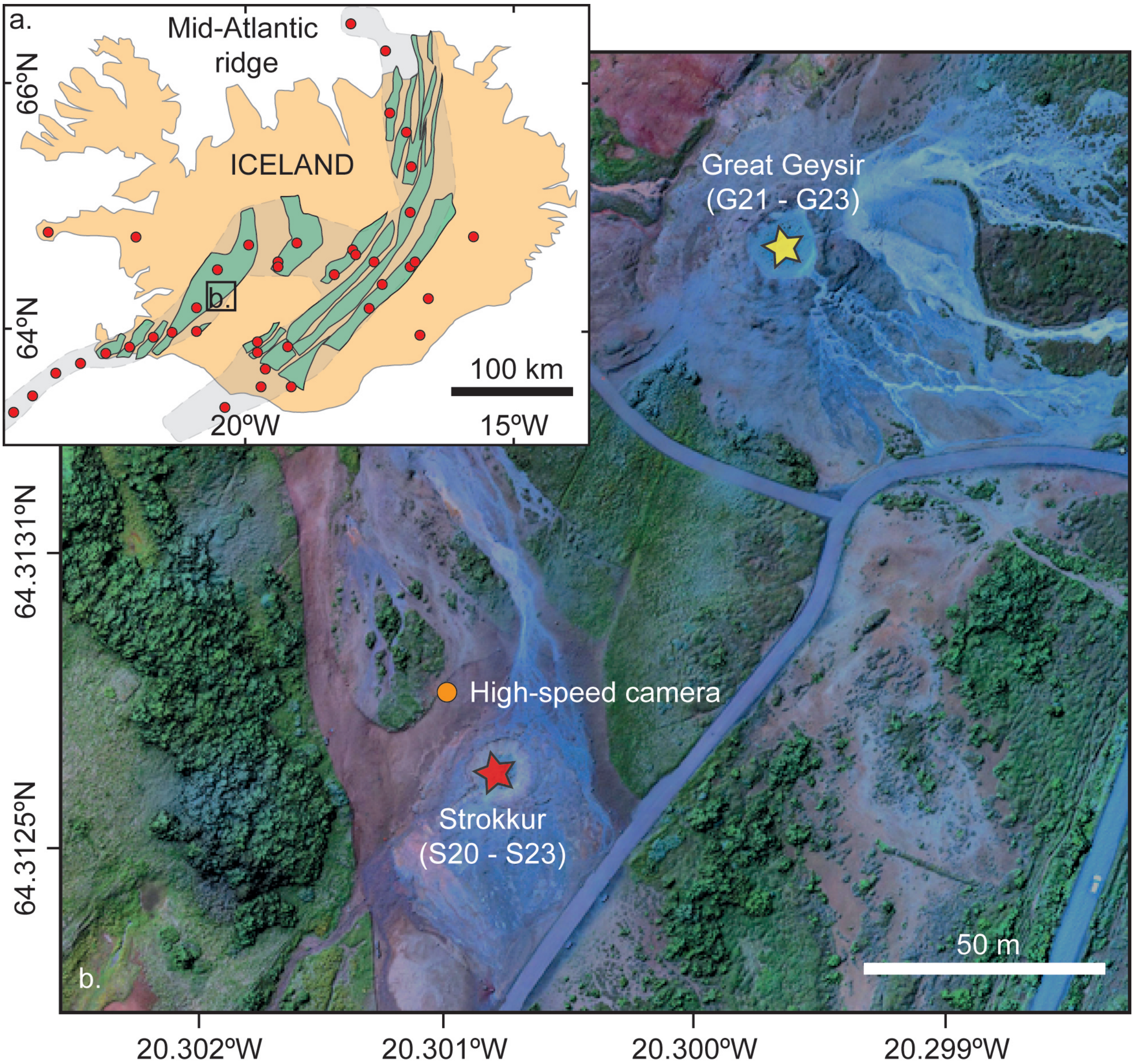


**Figure 1.** a. Map of Iceland showing the main volcanoes (red dots) and volcanic systems (green) associated with the mid-Atlantic ridge (light grey) and the geographic position of the field area (black square). b. Photo of part of the Haukadalur hydrothermal field reconstructed from images acquired with a drone showing the position of Great Geysir (yellow star) and Strokkur (red star). Distance between both geysers is about 110 m. Modified from Lupi et al. (2022).

0.25 to 0.75°C for the recorded temperatures (∼80-120°C). The response time of the sensor is not linear but consistent for both sensors and the temperature variations that we tested (Fig. 2. The response curve was fitted based on laboratory experiment of water temperature measurements at stabilisation times ranging from 1 to 20 minutes (see Supplementary Material for further details). The sensors record 63.2%, 90% and 99.8% of the temperature variation after 80, 160 and 300 s, respectively. However temperature inversion are instantaneously recorded. Therefore, the timing of temperature minima and maxima inside the geysers is correctly captured but the actual amplitude of the temperature variations is underestimated if the period between minima and maxima is lower than 300 s. Sampling rate was set to 1 Hz. Date and time of the selected temperature records that are analysed in this study are reported in Table 1, along with the estimated depth of the sensors. Further in the text, we refer to the temperature records of Strokkur's conduit on the $20^{th}$ of June at 9 m and 16 m and on the following nights as S20a, S20b, S21, S22 and S23, respectively. The temperature records in Great Geyser between $21^{st}$ and $23^{rd}$ June are also referred to as G21, G22 and G23 (Table 1). Analyses and processing of the temperature records were performed with MATLAB 2016a. Temperature raw data and processing scripts can be found in **?**. Before all analyses, the original temperature records were detrended to remove any potential instrumental drift. In addition, they were normalised by their maximum magnitude for spectral analyses. In parallel with temperature recording, the activity at Strokkur was visually monitored to obtain information on eruption characteristics and timing (using a GPS clock). In this work, we define as an eruption the water jet exiting the pool of the active geyser (i.e. Strokkur). Higher-order eruptions consist of sequences of water jets occurring at interval shorter than 46 s (according to the observation of Eibl et al. (2021)). The order of an eruption (double, triple, ...) is given by the number of water jets in the sequence. Within a continuous water jet, we distinguish pulses (rapid increases in exit speed associated to flow bursts), which are spaced by a few s or less, and occur within a continuous jet.

High-speed videos were recorded on selected eruptions at a resolution of 700 fps and 512 x 800 pixels using a Phantom MIRO camera connected to AF Micro-Nikkor 35 mm f/2.8D lens at a distance of about 10 m from Strokkur's vent. We captured 14 explosions (Table 2). Recording was manually started and set to save 700 images before onset. Recorded image sequences began as soon as the free water surface started rising. Because of low light and/or vapour covering the vent area, three movies started a few ms after the explosion onset. Maximum recording time was limited by the capacity of the internal hard drive of the camera, corresponding to up to 4 s duration of the movies at the set recording speed. Transfer of data of a single recording to an external hard drive required about 5 min, thus recording sequences of eruptions (i.e. higher-order eruptions) was not possible. Movies were analysed using the FIJI software (Schindelin et al., 2012) to measure explosion timing and vertical exit speeds. Images were calibrated based on the internal vent diameter as seen along the image plane and confirmed by drone images depicting the recording station. Eruption duration was calculated as the time between onset and end of emission of the steam and water jet. Duration estimations have uncertainties of 1/fps=1.4 ms. Vent diameter was measured based on aerial images acquired on a 20 Mpx camera mounted on a quadricopter (Phantom 4 Pro) flying at 65 m of altitude. We reconstructed a DTSM and an orthomosaic of the

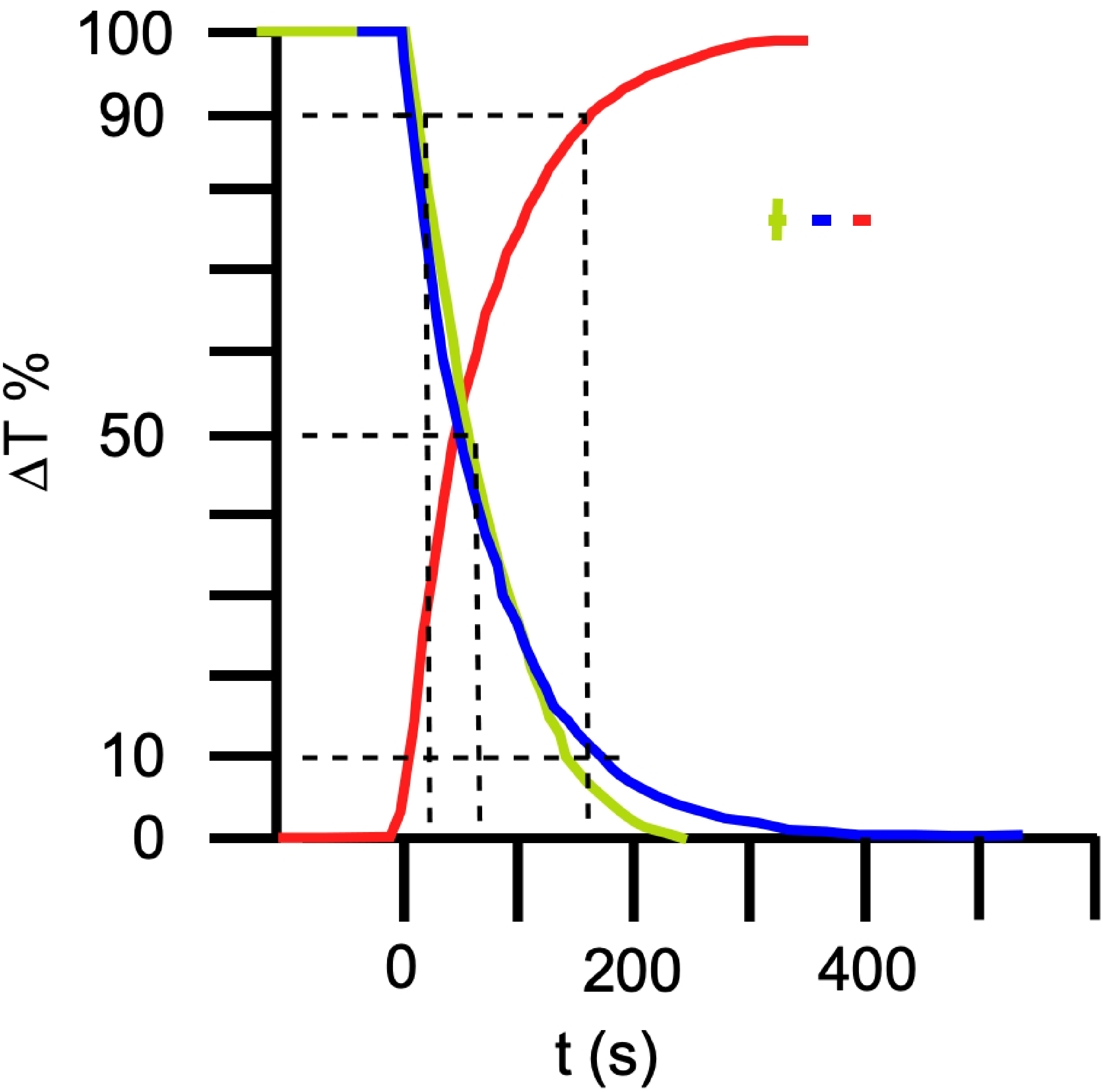


**Figure 2.** Response curve of the Hobo sensor to instantaneous temperature variation. The response curve is normalised to the temperature difference. Lateral cross/bars represent measurement errors of the same color curve.

| Recording | Conduit | Depth (m) | Start date | End date | Temperature (°C) | | | | |
|---|---|---|---|---|---|---|---|---|---|
| | | | | | mean | std | min | max | median |
| G21 | Geysir | 5±2 | 21/06-00h26'39" | 21/06-03h38'19" | 75.4 | 0.62 | 73.7 | 77.1 | 75.4 |
| G22 | Geysir | 5±2 | 22/06-00h02'29" | 22/06-02h51'59" | 66.7 | 0.98 | 64.9 | 68.9 | 66.7 |
| G23 | Geysir | 5±2 | 22/06-21h59'39" | 23/06-02h13'19" | 74.9 | 0.73 | 73 | 76.7 | 74.9 |
| S20a | Strokkur | 9±1 | 20/06-01h28'19” | 20/06-04h11'39” | 100.0 | 2.35 | 93.4 | 106.8 | 100.5 |
| S20b | Strokkur | 16±1 | 20/06-01h28'19” | 20/06-04h11'39” | 113.0 | 3.06 | 102.7 | 119.1 | 113.1 |
| S21 | Strokkur | 6±1 | 21/06-00h26'39" | 21/06-03h38'19" | 90.2 | 1.46 | 82.8 | 94.3 | 90 |
| S22 | Strokkur | 10±1 | 22/06-00h02'29" | 22/06-02h51'59" | 104.2 | 2.31 | 97.7 | 110.5 | 104.3 |
| S23 | Strokkur | 11±1 | 22/06-21h59'39" | 23/06-02h13'19" | 106.8 | 2.88 | 96.6 | 112.6 | 107.1 |

**Table 1.** Characteristics and basic statistics of the temperature records measured inside Great Geysir's and Strokkur's conduits. Depth is given with uncertainty. See method section and Supplementary Material for further details.

area (Fig. 1). Shooting produced 417 pictures with 75% of both front and side overlap. 10 markers were placed and measured with a kinematic GPS to reduce the error of the reconstruction. After the Structure from Motion processing with Agisoft Metashape©, we obtained an orthomosaic with a resolution of 1.6 cm/px and a DTSM of 3.2 cm/px. Uncertainty on spatial estimations is quantified by combining camera and mapping resolution (table 2). Thermal videos were captured at a position adjacent to the high-speed camera, in parallel with some explosions on June 18 (Table 2) using a Flir Duo R with a 160 x 120 IR sensor thermal camera recording at 25 fps. Apparent temperatures were calculated by setting emissivity to 0.95.

| Explosion | Date | Resolution ($m^{-2}$) | Duration (s) | Vertical exit speed (m/s) $1^{st}$ pulse | $2^{nd}$ pulse | $3^{rd}$ pulse |
|---|---|---|---|---|---|---|
| 1* | 18/06/2018 | 1.7 | >1.8 | 20.5 | 9 | - |
| 2* | 18/06/2018 | 1.4 | 2.5 | 15.2 | 24 | 3.3 |
| 3 | 18/06/2018 | 1.3 | 2.3 | 13.3 | 11.1 | - |
| 4 | 19/06/2018 | 1.2 | 1.7 | 13.3 | 20.7 | 9.9 |
| 5 | 19/06/2018 | 3.1 | 1 | 9.4 | 28.6 | - |
| 6 | 19/06/2018 | 1.3 | 1.5 | 4.4 | 7.9 | 12.1 |
| 7 | 19/06/2018 | 1.1 | 1.6 | 8.6 | 5 | - |
| 8 | 19/06/2018 | 1.1 | 1.9 | 7.6 | 12.8 | - |
| 9 | 19/06/2018 | 1.1 | 1.5 | 16.3 | 4.3 | 4.6 |
| 10 | 19/06/2018 | 1.1 | >3.2 | 9.2 | 8.7 | 3.6 |
| 11 | 19/06/2018 | 1.1 | >2.7 | 12.6 | 9.8 | - |
| 12 | 19/06/2018 | 1.1 | 2 | 14.2 | 10 | 3.2 |
| 13 | 19/06/2018 | 1.2 | 0.9 | 28.3 | - | - |
| 14 | 19/06/2018 | 1.2 | >2 | 12.3 | 30.6 | 6.5 |

**Table 2.** Eruptions captured by high-speed (700 fps) imaging records. * Eruptions recorded also with thermal cameras.

# 4 Results

## 4.1 Temperature records at Great Geysir and Strokkur

Temperature at Great Geysir was recorded at 5±2 m depth. The sensor was likely placed in the portion of the conduit just before it narrows down and we recorded the temperature variation at the pool/conduit limit (Fig. 3). However, while G21 and G23 display comparable average temperatures, G22 presents an average temperature about 8°C lower (Fig. 3a, Table 1). Yet, Walter et al. (2020) measured a steady temperature of ∼90°C from the surface down to 10 m below water at Great Geysir. A temperature profile measured in the 80's also showed a steady temperature of ∼80°C in the first 7 m, followed at depth by a progressive increase (Torfason, 1985; Pasvanoglu, 1998). We associate the temperature decrease of G22 to temporary cooling of the shallow system associated with rain that occurred during the recording. This hypothesis is supported by weather data collected at the two closest meteorological stations (see Supplementary Material for further details). Our measured temperatures are in the lower range of previously recorded temperatures for Great Geysir: up to 90°C at one metre water depth in 2016 and down to 73°C at the surface in 1998 (Pasvanoglu, 1998; Walter et al., 2020).

Water temperature in Strokkur's conduit are positively correlated with the estimated depth (Table 1, Fig. 3b). Weather data collected at the nearby stations show correlation with the water temperature at Strokkur (see Supplementary Material), confirming that the variations observed between the different nights reflect changes in the sensor depth. We measured at the surface of Strokkur a similar temperature than the previous records of 2016-2018 (Walter et al., 2020; Eibl et al., 2020). Considering the thermal gradient measured by Walter et al. (2020), our depth estimates are consistent with the corresponding recorded temperatures within the uncertainty range (i.e. 1 m).

### 4.2 Interpretation of temperature oscillations within Strokkur's and Great Geysir's conduits

The amplitude, frequency and shape of thermal oscillations vary between Great Geysir and Strokkur. Despite its quiescence, Great Geysir displays quasi-symmetrical oscillations with an amplitude of 1-2°C, that is similar across the surveys we performed (G21, G22 and G23, Fig. 3a). The largest amplitude oscillations (> 1°C) may be separated by a few minutes of steady conditions, with temperature variations in the range of the instrument resolution. These periods of steady conditions can be seen for example between 95 and 102 min on G22 or between 188 and 202 min on G23 (Fig. 3a). However, sensors registered large temperature oscillations in Strokkur at a frequency of the same order of the sensor response time (i.e. $10^2$ s).

Temperature oscillations recorded at Strokkur are more regular and asymmetrical with a generally larger amplitude (up to 15°C) than those recorded at Great Geysir (Fig. 3b). The amplitude of temperature oscillations and their mean value increase with the sensor depth (Table 1). The shape of oscillations also varies between the different records. The shallowest record, S21, displays asymmetrical oscillations, with smoother temperature decays than rises (Fig. 3b). The oscillations (i.e. peaks and low) are much less marked than for the other records of Strokkur and are sometimes interrupted by short periods (2-3 min) of steady conditions, with temperature variations within the instrument resolution, as observed for Great Geysir. The deepest record, S20b, displays asymmetrical oscillations, with smoother temperature rises than decay (Fig. 3b). The temperature rises of S20b are also marked by high-frequency and minor amplitude oscillations (blue line in Fig. 4). Temperature records around 10 m depth (S20a, S22 and S23) show less asymmetrical oscillations than S21 and S20b (Fig. 3b) and the high-frequency oscillations in the temperature rises are less marked than for S20b (black line in Fig. 4).

We set a thermal cycle as the oscillation between two temperature maxima. Each cycle comprises a cooling phase, between the maximum and minimum, and a warming phase between the minimum and maximum (see Supplementary Material for further details) The spectrograms of the temperature records at Great Geysir highlight a main frequency peak between 1 and 2 mHz (Fig. 5a). The 1-2 mHz frequency range has a corresponding period of 8 to 16 min, which is consistent with the duration of the thermal cycles at Great Geysir (Table S2 in Supplementary Material). Spectrograms of the synchronous S21, S22 and S23 records show distinct patterns (Fig. 5b). They all present a frequency peak between 1 and 2 mHz, the power/frequency of which varies during the recording time. It intensifies between 1.4 and 2h and between 1h and 1.5h for S22, as well as between 2h and

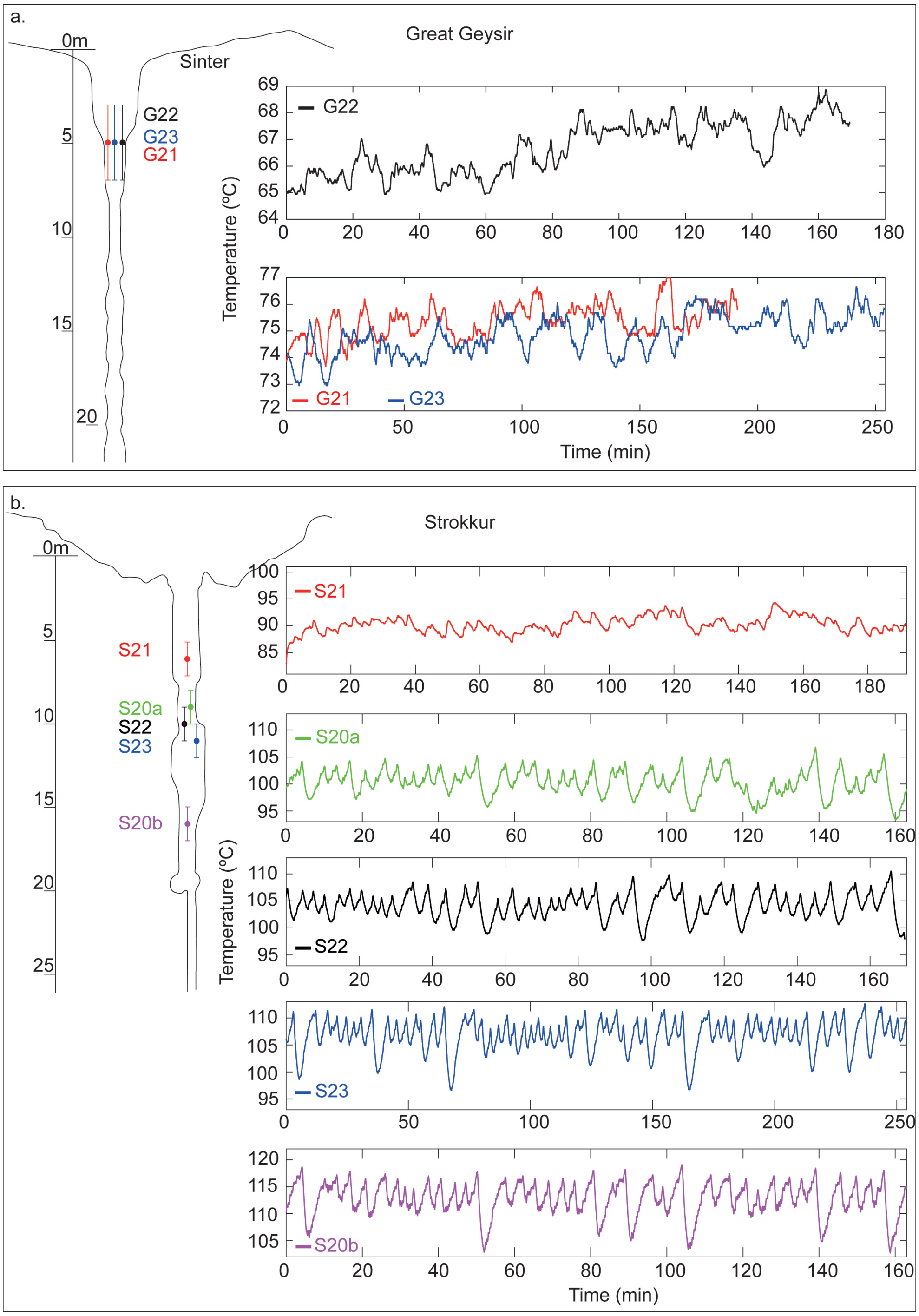


**Figure 3.** Schematic representation of the conduits with the temperature records inside Great Geysir (a) and Strokkur (b) during the nights $20^{th}$ - $23^{rd}$ June 2018. The records depth and associated uncertainty are represented inside the conduits (left) by a dot and error bar, respectively, using the same colour code than the data (right). S20a, S22 and S23 are presented in the same panel because given the 1 m uncertainty, we can consider they were recorded at the same depth. The conduit shapes are taken from Eibl et al. (2021) and Torfason (1985) (reported also in Pasvanoglu (1998)) for Strokkur and Great Geysir, respectively.

Figures/paper/Fig4_Night20.jpg

**Figure 4.** Temperature recorded during the $20^{th}$ June 2018 at 9 m (black line, S20a) and 16 m (blue line, 20b).

Figures/paper/Fig5_Power_spectrum.jpg

**Figure 5.** Normalised signals and associated spectrograms of temperature recorded inside Great Geysir (a) and Strokkur (b).

3h for S23. These periods record larger amplitude and longer periodicity oscillations in the temperature records (Fig. 5b). Another dominant frequency around 4 mHz is visible on the S22 and S23 spectrograms. (Fig. 5b). Its corresponding period of 4.2 min is consistent with the duration of the thermal cycles at Strokkur (Table S3 in Supplementary Material).

### 4.3 Strokkur's eruption and temperature variation

To compare the geysering activity with the temperature records, we visually monitored the eruptions at Strokkur during the nights of $22^{nd}$ and $23^{rd}$ June and recorded the timing (with a gps calibrated clock) of 78 jets, as well as the time interval between them. Based on previous work (Eibl et al., 2020), jets erupting within less than 46 seconds are expected to belong to the same eruption of higher-order (double, triple, etc).

We thus witnessed 49 single, 10 double and 3 triple eruptions (grey areas in Fig. 6a,b). We did not observe higher-order (i.e. 4, 5 or 6) eruptions as reported by Eibl et al. (2020). We note a correlation between the eruptions and maxima of synchronous temperature records (Fig. 6a,b). All observed eruptions coincide, within a timing uncertainty of a few s, with most temperature maxima associated with an eruption (Fig. 6c,d). Only two small temperature peaks around 23h39 and 01h44 (black triangle in Fig. 6b) during our monitoring could not be linked to a visible explosion at the surface. However, we also occasionally observed a bulge of the water table. The water table returned to its original level and was not followed by a water jet as this would typically happen during an eruption. This phenomenon was previously described at Strokkur and referred to as *aborted eruption* (Eibl et al., 2020; Walter et al., 2020). The temperature maxima of double and triple eruptions are reached just before the last water jet (Fig. 6c,d). Based on these observations, we conclude that an eruptive cycle coincides with the thermal cycle (Fig. **??**). The length of the thermal cycle corresponds to the time interval after eruption (TAE) of Eibl et al. (2020).

Based on our direct observations, we distinguish between thermal cycles following eruptions of different orders(Fig. 7). Further statistics for this analysis are reported in the Supplementary Material. We characterise the temperature evolution at 10 m depth within Strokkur's conduit during the cooling and warming phases of the eruptive cycles, as S22 and S23 were recorded at the same depth given the uncertainty. The duration of the thermal cycles increases with the eruption order (Fig. 7a). We observe that the recorded temperature variation for both the cooling and warming phases increase with the eruption order from ~4.5°C for single to ~13.5°C for triple eruptions (Fig. 7b). The temperature profiles show a distinct negative incursion after double and triple eruptions that is more pronounced than for single eruptions (Fig. 6). For the considered triple eruptions, the temperature variation is on average larger for the cooling than the warming phase. The duration of both cooling and warming phases after the eruption increases with the eruption order; but this increase is larger for the warming than the cooling phase (Fig. 7c). The cooling phase lasts on average 1.6±0.8, 2.4±0.3 and 2.8±0.4 min for single, double and triple eruptions, respectively. The warming phase lasts on average 2.1±0.8, 4.4±1.4 and 5.8±1.8 min for single, double and triple eruptions, respectively. However, the actual temperature variations need to be calibrated based on the sensors' response curves. Considering an almost instantaneous temperature drop associated with the eruption discharge and the recorded duration of the cooling phases, we estimate that the sensors recorded about 70%, 85% and 90% of the temperature drop for single, double and triple eruptions during the cooling phase, respectively. The estimated temperature drop experienced inside Strokkur at ~10 m depth would thus be about 6.2, 11.5 and 15.5°C for single, double and triple eruptions, respectively. The more complex pattern of temperature rises recorded by the sensors (Fig. 6) could hardly be explained by an instantaneous temperature rise. Therefore, a calculation of the real temperature variation during the warming phase would not be accurate.

Based on direct observations, all records excepting S21 show clear oscillations that can be used as proxy for eruption identification. A few selected peaks could correspond to aborted eruptions, but based on our monitoring, we assume that their number is statistically irrelevant. We analyse the synchronous S20a and S20b

Figures/paper/Fig6_Teruption.jpg

**Figure 6.** Temperature variation and eruptions at Strokkur. a. S22 and b. S23 records. c. and d. zooms in S23 record. Orange vertical lines: single eruptions. Red vertical lines: jets of double eruptions. Blue vertical lines: jets of triple eruption. Black triangle: aborted eruptions. Grey areas: period of visual monitoring of Strokkur's activity. Yellow area: selected data shown in panels c. and d.

Figures/paper/Fig7_analyse_obs_eruption.jpg

**Figure 7.** Analyse of observed eruptions. a. TAE (time after eruption) of observed single, double and triple eruptions. b. Temperature variation ($\Delta$T) and c. associated period ($\Delta$t) for the warming (red) and cooling (blue) phases of eruptive cycles and for single, double and triple eruptions. Mean value (triangle or circle) and standard deviation (error bars) are reported in the graphs for the recorded temperature and time. The real temperature drops, estimated from the response time curves are shown in b. by the blue asterisks. Statistics of the analysis are presented in Table S4 of the Supplementary Material.

records to provide a direct comparison of the temperature evolution during eruptive cycles at different depths (Fig. 4). We first select automatically minima and maxima, and manually correct eventual missing/inserted peaks after visual inspection to obtain the same number (and synchronous) eruptions between S20a and S20b. Because of their larger temperature variation and TAE, higher order eruptions (double and triple) were identified based on the strongest negative incursions in S20b (Fig. 4). S20a being recorded within the same depth range than S22 and S23, we then use the results of the previous analysis to discriminate between double and triple eruptions. We conservatively considered that triple eruptions should satisfy the two following criteria: a TAE $>$ 408 sec and a $\Delta$T for the cooling phase $>$ 11°C. The TAE threshold corresponds to the mean value minus one standard deviation of the TAE of triple eruptions documented by Eibl et al. (2020). We found best to use this value as the TAE was estimated on a much larger sample of eruptions. The threshold of 11°C for the temperature variation is equivalent to the mean value minus one standard deviation of the temperature variations for triple eruptions (considering both cooling and warming phase). Note that this threshold is determined here based on our recorded temperature variations and not from the estimation of the real temperature drops. This is consistent here because the response time is similar regardless of the temperature variations or sensor, but the threshold should have to be reevaluated in future studies based on the response time of the employed sensor. We could not identify any triple eruption. The temperature variation of both the cooling and warming phases increases with depth for single and double eruptions (Fig. 8, left). For single eruptions, the mean recorded temperature variation is similar between cooling and warming phases and it increases from $\sim$4°C at 9 m depth to $\sim$6°C at 16 m depth (Fig. 8a, left). For double eruptions, the mean temperature variation is slightly higher in cooling than warming phases but it generally increases from $\sim$8.5°C at 9 m depth to $\sim$13°C at 16 m depth (Fig. 8b, left). The cooling phase is slightly shorter with depth, while the warming phase slightly lasts longer for both single and double eruptions (Fig. 8, right). The cooling phase lasts on average 1.6$\pm$0.7 min at 9 m depth and 1.1$\pm$0.3 min at 16 m depth for single eruptions, whereas for double eruptions it drops from 2.3$\pm$0.4 min at 9 m depth to 1.6$\pm$0.2 min at 16 m depth. The warming phase lasts on average 2.1$\pm$0.8 min at 9 m depth and 2.6$\pm$0.8 min at 16 m depth for single eruptions, whereas for double eruptions it increases from 4.3$\pm$0.8 min at 9 m depth to 5$\pm$1 min at 16 m depth (Fig. 8, right). Based on the sensor response times, we estimated that at 9 m depth, 70 and 85% of the temperature drop was recorded for single and double eruptions, respectively, whereas at 16 m, only 55 and 70% of the temperature drop was recorded for single and double eruptions, respectively. The actual temperature drop after single eruptions would thus be of 5.5 and 10.2°C at 9 m and 16 m depth, respectively. It is estimated at 10.4 and 19.4°C at 9 m and 16 m depth after double eruptions, respectively.

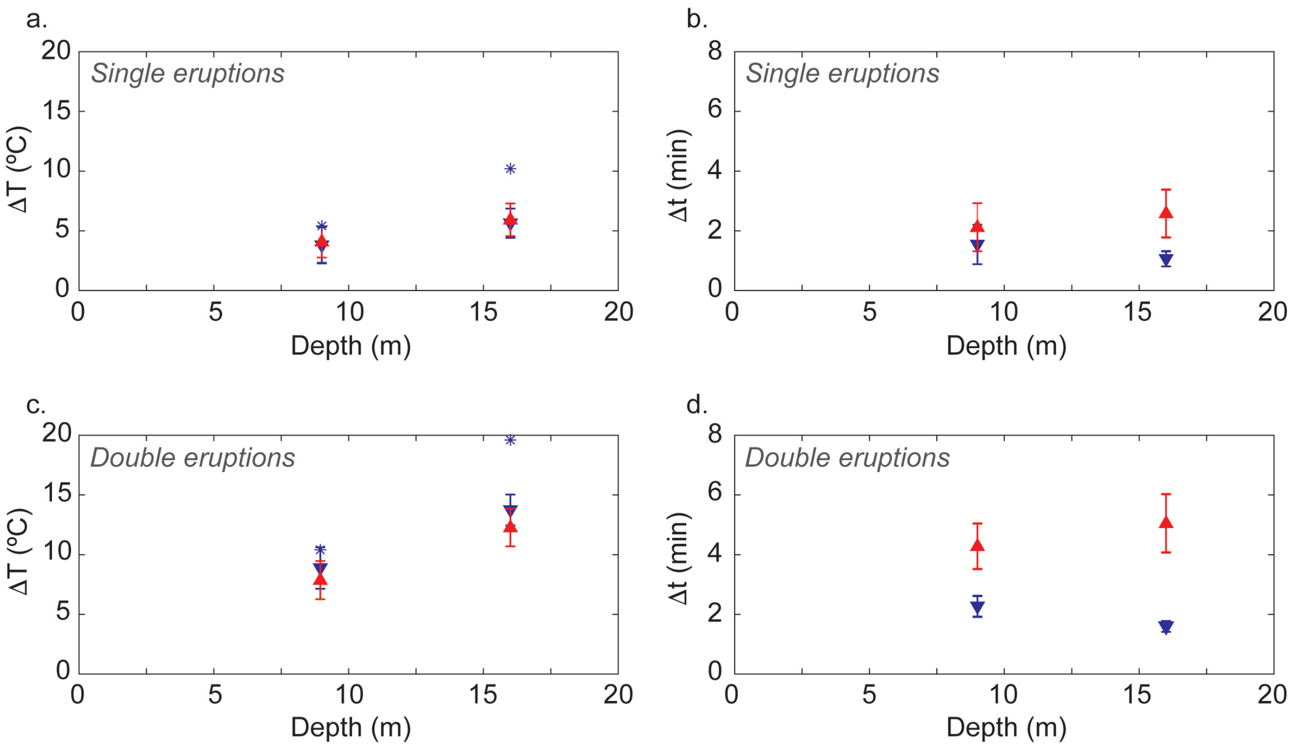


**Figure 8.** Analysis of eruptions. Temperature variation (ΔT) and associated period (Δt) for the warming (red) and cooling (blue) phases of single (a.) and double (b.) eruptions at different depths. Mean value (triangle or circle) and standard deviation (error bars) for the recorded temperature and timing are reported in the graphs. The real temperature drops, estimated from the response time curves are shown in the left panels (a. and b.) by the blue asterisks. Selected minina and maxima and statistics of the analysis are presented in Figure S6 and Table S5 of the Supplementary Material.

### 4.4 Single eruption dynamics

Further information on eruption dynamics was obtained from high speed recordings of the single explosions listed in Table 2, whose duration ranges from 1.5 to >3 s. These eruptions were always anticipated by a bulging of the water free surface atop the vent, and rapidly followed by the rise of a turbulent vapour pocket which eventually broke the liquid film and started a vertical jet of mixed vapour and water droplets. The free liquid surface rose above the vent at speeds generally <1 m/s, while the speed of bubble rise, as it emerged above the vent and reached the top of the bulge, ranged from 1 to 4 m/s. The initial pulse was followed in most jets by a faster second pulse at 0.7 ± 0.3 s after the first one. About half of the eruptions ended with the second pulse, while the remaining ones were marked by a third, low-energy pulse following the second one after 0.5 ± 0.5 s (Fig. 9). Finally, one eruption showed a fourth pulse, occurring at 0.9 s after the third one (Fig. 9). The initial pulse was ejected at exit speeds ranging from 5 to 28 m/s. Measured speeds of the jet associated with the second pulse range from 4 to 30 m/s. The jet associated with final and third pulses are generally < 10 m/s. Water from the jet fell almost completely back into the conduit pool, except for the fine spray which was dispersed in the atmosphere. Because of their typically larger ejection speed and similar duration with respect to the other pulses, we assume that most of the mass is released during the second explosion pulses. Few eruptions have shown that bulging before eruption was clearly associated with the rise of multiple bubbles each occupying a portion of the conduit. Thermal videos recorded water jet temperatures at the vent of 68-72°C. This agrees well with the most superficial temperatures measured in the conduit. No significant temperature difference was noted among pulses within the same eruption. We also occasionally observed "aborted eruptions" ((Eibl et al., 2020; Walter et al., 2020)): a bulge of the water table, but without the subsequent eruption and the formation of a water jet, as this would typically happen during an eruption. The bulge then collapsed on itself and the water table returned to its original level.

## 5 Discussion

### 5.1 Analysis of temperature oscillations

By convention an eruptive cycle starts with the onset of an eruption (Kieffer, 1984). In our study we use the temperature data as a proxy to identify eruptive cycles of Strokkur, assuming that the temperature maxima coincide with the eruptions. This assumption is less accurate for higher-order eruptions, because the temperature peak does not coincide with the first but the last water jet of a sequence.This will slightly overestimate duration and amplitude of the warming phase of the previous eruptive cycle. Further deviations could also occur when estimating the phase duration from automatic selection of minima and maxima if a temperature plateau is present. They are usually present around both minima and maxima and last between 5 and 10 sec. As a result, there is an uncertainty of a few s to the estimation of the duration of the eruption phases.

We could not capture the true temperature pattern during an eruptive cycle because of the response time of the sensors (Fig. 2). Yet, temperature inversions were accurately captured, allowing reliable quantification

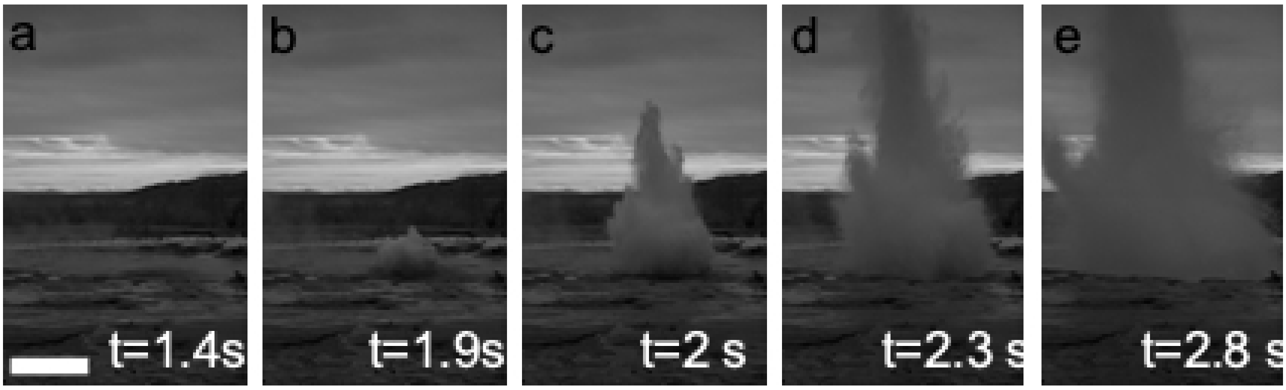


**Figure 9.** Type dynamics of eruption jet at Strokkur. Scale bar is 3 m long. a) initial bulging, b) break up of the free surface, c) initial jet d) rising jet formed by multiple spikes) e) second pulse while the first jet is already collapsing e) third small pulse covered by fallout of previously ejected water

of the duration of the cooling and warming phases. We assumed an instantaneous temperature drop after the eruption to estimate its actual value from the response time curve. This assumption implies that most of the energy will be released during the eruption. In any case, the temperature variations are significantly different between the eruption types (at least 4 to 5°C after correction) or the recording depth to reflect a variability inside Strokkur's conduit and not a recording bias. We observe that the temperature variations increase with depth and the eruption order in a similar manner for both the warming and cooling phases. However, the phase duration increases with the eruption order significantly more for the warming than cooling phases. Moreover, the phase duration slightly increases with depth for the warming phase while it decreases for the cooling phases, changing the shape of the oscillation from symmetrical to asymmerical.

We identified and analysed the oscillations for 107 single, 21 double and 4 triple eruptions from the S20a, S22 and S23 records. Unless two higher-order eruptions follow each other (it only happened once), the period between two temperature maxima corresponds to the TAE defined by Eibl et al. (2020). We observed TAEs of 3.7±1, 6.5±1.2 and 8.8±1.7 min for single, double and triple eruptions, respectively. These values are in good agreement with previous TAEs measured by Eibl et al. (2020) and attest of the regularity of Strokkur's eruptions. The analysis on the temperature oscillations yields similar results to the one shown in Figure 7. The mean values remain almost the same but the standard deviations are reduced for both single and double eruptions due to a larger dataset (see Figs. S7, S8 and Table S6 in Supplementary Material). In absence of synchronous seismic data or camera monitoring the water surface, the identification of the eruption type from the temperature data cannot be absolutely certain. We are confident that the largest temperature oscillations are associated with higher-order eruptions, but a few double eruptions could have been misidentify as single eruptions if their temperature variation and TAE were in the lower range for double eruptions. The number of observed double (11) and triple (3) eruptions is statistically too low to obtain reliable discriminating criteria between double and triple eruptions. In addition, the sensors recorded a minimum and not the actual temperature drop, which implies that the discriminating threshold of between double and triple eruptions for the temperature variations is not accurate. In any case, we consider the dataset of single eruptions as statistically representative. Our study highlight significant trends for the temperature variations between the different types of eruptions and the recording depths. Future studies could evaluate the true temperature variations during the eruptive cycle with sensors possessing a quasi-instantaneous response time. These studies should also consider a synchronous seismic recording and camera monitoring of the water surface to properly capture the temperature variation with respect to the eruptive cycle and its different phases.

### 5.2 Heat transfer and mass flow in Strokkur conduit

Eibl et al. (2021) recognised four distinctive phases in the seismic signal recording an eruptive cycle of Strokkur: 1) eruption, 2) post-eruptive conduit refilling, 3) gas filling of the bubble trap, and 4) bubble collapse. Identifying these four phases in the temperature records is, however, difficult because the water temperature logs reflect different processes (heat transfer and mass flow) and conditions with respect to the seismic oscillations (ground motions associated with wave formation and propagation). We propose a complementary model of conduit dynamics based on the temperature oscillations. Each eruption is followed by a temperature decay and a subsequent temperature increase that we refer to as conduit cooling and conduit warming phases, respectively, to avoid any confusion with the terms 'charging' and 'discharging' phases that commonly refer to bubble trap processes.

As Eibl et al. (2021) suggest, vapour accumulates at depth within a fixed volume chamber (the "bubble trap") connected with the conduit. The amount of vapour leaving the bubble trap is controlled by the local small temperature and pressure variations in the bubble trap and conduit. The bubble trap modulates gas release based on heat transfer rate (which controls vapour production), its volume (which controls pressure) and the geometry of the neck connecting it to the main conduit (which are associated with periodic emptying and refilling). As bubbles are released from the trap, they rise in the conduit and eventually coalesce into a slug-like structure (Wallis, 1969) leading to a single eruption or, alternatively (if the neck is large enough, as demonstrated by Davidson & Schüler, 1960; Vergniolle & Jaupart, 1986), a slug is directly formed at the bubble trap exit. Our visual evidence from high speed imaging at the vent suggests that each eruption is fed by a slug rising in the conduit and generating a series of eruptive bursts. Higher-order eruptions are then associated (Fig. 3) to multiple successive releases of vapour from the trap that creates spaced slugs (Vergniolle & Jaupart, 1986), which eventually results in sequences of explosions. This model for slug formation implies similar transient dynamics associated with each cycle/eruption. Each transient is marked by the rise of a mass of vapour through stagnant water filling the conduit. During rise, the slug is expanding according to the hydrostatic pressure gradient. Its drift velocity is proportional via the flow Froude number (Fr) to the square root of gravity and conduit diameter (E. White & Beardmore, 1962). Given that Fr is constant for the condition expected in Strokkur (Wallis, 1969) any slug velocity fluctuation and a final acceleration are only due to irregular conduit geometry and uppermost widening (Fig. 3, Walter et al., 2020), but will be constant among different eruptions, depending only on conduit but not on the volume of the vapour released. For the conditions expected at Strokkur, and the conduit diameter we are expecting a Fr of 0.56 (Viana et al., 2003) and slug rise velocity of the order of $10^0$ m/s. The rise of the slug in stagnant water will be accompanied by formation of a wake of recirculating water behind it. The dynamics and length of the wake will depend on the balance between viscous and inertial forces as quantified by the dimensionless inverse viscosity number, corresponding to the ratio between the slug velocity multiplied by the conduit diameter and water viscosity (Nogueira et al., 2006). Again, for the conditions expected in the conduit at Strokkur, inverse viscosity is much larger than $10^3$ and thus water (re-)circulation in the wake will be turbulent. The wake is expected to be up to ten times longer than the slug (Pinto et al., 1998). Within a single eruption, we associate the first pulse of the water jet with ejection of the the water dragged by the slug (the liquid film above the bubble) and successive pulses as due to the wake ejection and eventually to steam flashing in the conduit. The highest exit speeds are reached during wake emission (second pulse). We notice that this is a very different dynamics with respect to Strombolian explosions, which are also due to the rise of gas slugs in a stagnant liquid (magma). In Strombolian explosions, because of the higher viscosity of the magma, the slug wake will be shorter and marked by laminar dynamics; the maximum ejection velocities are attained in the initial phase followed by steady emission of the wake material (Gaudin et al., 2014; Pioli et al., 2022). Slug rise will be mostly recorded by pressure fluctuations (Azzopardi et al., 2014), but also by a discontinuity in the temperature rise due to the passage of the wake, which is kept in internal thermal equilibrium by internal liquid (re-)circulation (van Hout et al., 2002; Shemer et al., 2007). The temperature drop during the conduit cooling phase is associated with mass transfer: i) evacuation of water and vapour associated with the eruption and b) filling of the conduit by phreatic water through fractures and water cooled in the jet falling back in the vent. This results in a more dramatic temperature decay at depth with respect to the shallow conduit, because of the water temperature gradient in the conduit and the more uniform temperature of phreatic water (Lupi et al., 2022). In parallel, duration of the conduit cooling phase decreases with depth. The conduit warming phase has a more complex pattern, being marked by one or more discontinuities in the curve (Fig. 3b, Fig. **??** and Fig. S5 in Supplementary Material) in all records except for S21 (the shallowest).The discontinuity records a short (1-5 s) disturbance (in the form of a plateau), which could be associated with the passage of the vapour mass and its associated (re-)circulation turbulent wake. Unfortunately, the sampling rate and sensor response time were not accurate enough to record the internal dynamics of this structure. The general shape and slope of the heating ramps are controlled by heat transfer rates from the deep source (bubble trap?) to the mass of water filling the conduit and are independent from depth. We notice that in higher order eruptions, which are marked by a sequence of two or more water jets, our sensors did record only a 'simple' conduit cycle. One possible reason is that the sensors accuracy did not allow for identification of very short warming/cooling phases; otherwise, single jets in a sequence are smaller (i.e involve smaller masses of water) than single eruptions: the conduit is emptied only partially with no breakup of the warming cycle. However, the TAE increases linearly with the eruption order, consistently with a constant heat supply from depth, Eibl et al. (2020).

### 5.3 Periodicities of thermal oscillations

Strokkur's temperature spectrograms are consistent with the eruptive dynamics. The 4 mHz frequency, coinciding with the average period of the oscillations of S20a, S20b, S22 and S23 (see Table 3 in Supplementary Material) highlights the overall eruption periodicity, whereas the 1-2 mHz frequency range relates to the occurrence of double or triple eruptions in the same periods (Figs. 5,6). Temperature oscillations at Great Geysir are not synchronous nor display similar shapes with respect to those recorded at Strokkur. No cross-correlation between Great Geysir and Strokkur temperature signals could be established. A recent geo-electric survey suggested that both geysers would be connected at depth to a same reservoir by a network of fault and fractures (Lupi et al., 2022). However, deep signals are likely modulated by the complex geometry of this connection, hampering any synchronicity in the temperature records. Great Geysir's thermal spectrum is missing the 4 mHz peak, suggesting that the general Strokkur's eruption dynamics (and associated energy releases) do not affect Great Geysir and likely the general system. The 1-2 mHz frequency peak is instead observed on the spectrograms of both Great Geysir and Strokkur, although they are shifted in time (Fig. 5). This suggests that this frequency component, also associated with higher order eruptions at Strokkur, might be associated with deep seated processes, or alternatively, that larger energy discharges of the Strokkur system could also have an effect on Great Geysir dynamics. Our measurements cannot explain the observed eruption periodicity, which is controlled by source dynamics: steady conditions in the experimental period and also across the previous year (Eibl et al., 2020) do not allow any accurate modeling of the source parameters nor the bubble trap capacity.

## 6 Conclusions

We documented for the first time the fluid temperature evolution inside the conduits of the active Strokkur and the quasi-dormant Great Geysir geysers in the Haukadalur hydrothermal field, Iceland. The consistency of dynamics and frequency of Strokkur's eruptions allowed us to collect a representative dataset and the temperature evolution at different depths inside the conduit during several eruptive cycles. Periodicity of the temperature oscillations are associated with the eruptive dynamics and/or the general system dynamics that could also be retrieved in the conduit of Great Geysir, suggesting a deep (more than 100 m depth) connection between both geysers. At Strokkur we identified eruptive cycles for single, double and triple eruptions from its temperature records and visual observation of the eruptive activity. The time after eruption for our identified eruptions agrees with previous studies and between the different days of recording, confirming the regularity of Strokkur's eruptions. Based on the temperature records, we analyse the conduit cooling and subsequent warming phases that follow an eruption. After an eruption, the conduit is refilled by both water falling back from the jet in the pond and laterally from the shallow aquifer. In the meanwhile, new vapour accumulates in the bubble trap. Temperature rise is associated with heat transfer from depth, while temperature drop is due to conduit refill in the few seconds following the eruption from water falling back in the pool and feeding from the shallow aquifer. The temperature variations during the cooling phase increase with depth or with eruption type, showing faster heat transfer in the deeper part than in the shallow part of the conduit and larger heat release by higher-order eruptions. Eruptions consist in a series of vertical pulses of water and steam, emitted at speeds ranging from 4 to 30 m/s. They are preceded by the rise of the water table in the conduit until a large volume of steam breaks the free water surface and exits, dragging jets of water which partly fall back in the pond and partly fragment into a fine aerosol.

## Acknowledgments

We thank the Umhverfisstofnun, the Environment Agency of Iceland for the research permit at the Haukadalur hydrothermal field, and the park rangers for their support. O. Rögnvaldsson and G.N. Petersen are thanked for providing information about weather data. This study was partially funded by the Augustin Lombard Scholarship for S. Mueller, who is also thanked for his support in the field. We are grateful to G. Carrier for her help in the field and A. Mazzini for providing support with hardware. M. Collignon was funded by GENERATE (SNF project PYAPP24_66900, PI Matteo Lupi) and also by a Marie Skłodowska-Curie Individual Fellowship (NERUDA 793662). L. Pioli acknowledges the Fond National Suisse project 200021_162439. M. Collignon thanks Ø. Hammer, V. Antunes and T. Planes for fruitful discussions. The authors thank E. Eibl for her comments and suggestions on a previous version of this manuscript. All temperature data and matlab scripts to process them and generate the figures of this manuscript, as well as the figures and supplementary material have been placed in a zenodo repository under the DOI 10.5281/zenodo.7632693.

## References

Adelstein, E., Tran, A., Munoz-Saez, C., Shteinberg, A., & Manga, M. (2014). Geyser preplay and eruption in a laboratory model with a bubble trap [Journal Article]. *Journal of Volcanology and Geothermal Research*, *285*, 129-135.

Anderson, L., Anderegg, J. W., & Lawler, J. (1978). Model geysers [Journal Article]. *American Journal of Science*, *278*, 725-738.

Azzopardi, B., Pioli, L., & Abdulkareem, L. (2014). The properties of large bubbles rising in very viscous liquids in vertical columns [Journal Article]. *International Journal of Multiphase flow*, *67*, 160-173.

Belousov, A., Belousova, M., & Nechayev, A. (2013). Video observations inside conduits of erupting geysers in kamchatka, russia, and their geological framework: Implications for the geyser mechanism [Journal Article]. *Geology*, *41*(3), 387-390.

Bryan, T. (1995). *The geysers of yellowstone: Boulder, colorado* [Book]. University Press of Colorado.

Bunsen, R. (1847). Physikalische beobachtungen ueber die hauptsaechliche geysir islands [Journal Article]. *Poggendorffs Ann. Phys. Chem.*, *72*, 159-70.

Cros, E., Roux, P., Vandemeulebrouck, J., & Kedar, S. (2011). Locating hydrothermal acoustic sources at old faithful geyser using matched field processing [Journal Article]. *Geophysical Journal International*, *187*, 385-393.

Davidson, J., & Schüler, B. (1960). Bubble formation at an orifice in a viscous liquid [Journal Article].

*Transactions of the Institution of Chemical Engineers*, *75*, S105-S115.

Droznin, V., Bakhtiyarov, V., & Levin, V. (1999). Temperature measurements in the velikan geyser basin (valley of geysers, kamtchatka) [Journal Article]. *Volcanol. Seismol.*, *21*, 67-78.

Eibl, E. P., Hainzl, S., Vesely, N., Walter, T., Jousset, P., Hersir, G., & Dahm, T. (2020). Eruption interval monitoring at strokkur geyser, iceland [Journal Article]. *Geophysical Research Letters*, *47*, 1-10.

Eibl, E. P., Jousset, P., Dahm, T., Walter, T. R., Hersir, G. P., & Vesely, N. I. (2019). *Seismic experiment at the strokkur geyser, iceland, allows to derive a catalogue of over 70,000 eruptions.* [Dataset]. doi: doi:10.5880/GFZ.2.1.2019.005

Eibl, E. P., Müeller, D., Walter, T., Allahbakhsi, M., Jousset, P., Hersir, G., & Dahm, T. (2021). Eruptive cycle and bubble trap of strokkur geyser, iceland [Journal Article]. *Journal of geophysical research: Solid Earth*, *126*, 1-20.

Gaudin, D., Taddeucci, J., Scarlato, P., Moroni, M., Freda, C., Gaeta, M., & Palladino, D. (2014). Pyroclast tracking velocimetry illuminates bomb ejection and explosion dynamics at stromboli (italy) and yasur (vanuatu) volcanoes [Journal Article]. *Journal of geophysical research: Solid Earth*, *1119*, 5384–5397.

Hurwitz, S., Clor, L. E., McCleskey, R. B., Nordstrom, D. K., Hunt, A. G., & Evans, W. C. (2016). Dissolved gases in hydrothermal (phreatic) and geyser eruptions at yellowstone national park, usa [Journal Article]. *Geology*, *44*, 235-238.

Hurwitz, S., & Manga, M. (2017). The fascinating and complex dynamics of geyser eruptions [Journal Article]. *Annual Review of Earth and Planetary Sciences*, *45*, 31-59.

Hutchinson, R., Westphal, J., & Kieffer, S. W. (1997). In situ observations of old faithful geyser [Journal Article]. *Geology*, *25*, 875-878.

Ingebritsen, S., & Rojstaczer, S. (1993). Controls on geyser periodicity [Journal Article]. *Science*, *262*, 889-892.

Ingebritsen, S., & Rojstaczer, S. (1996). Geyser periodicity and the response of geysers to small strains in the earth [Journal Article]. *Journal of geophysical research*, *101*(B10), 21891-21907.

Jones, B., Renaut, R. W., Torfason, H., & Owen, R. B. (2007). The geological history of geysir, iceland: a tephrochronological approach to the dating of sinter [Journal Article]. *Journal of Geological Society, London*, *164*, 1241-1252.

Kedar, S., Kanamori, H., & Sturtevant, B. (1998). Bubble collapse as the source of tremor at old faithful geyser [Journal Article]. *Journal of Geophysical Research*, *103*(B10), 24283-24299.

Kieffer, S. W. (1984). Seismicity at old faithful geyser: an isolated source of geothermal noise and possible analogue of volcanic seismicity [Journal Article]. *Journal of Volcanology and Geothermal Research*, *22*, 59-95.

Kieffer, S. W. (1989). Geologic nozzles [Journal Article]. *Reviews of Geophysics*, *27*(1), 3-38.

Kiryukhin, A., Rychkova, T., & Dubrovskaya, I. (2012). Formation of the hydrothermal system in geysers valley (kronotsky nature reserve, kamchatka) and triggers of the giant landslide [Journal Article]. *Applied Geochemistry*, *27*, 1753-1766.

Lupi, M., Collignon, M., Fischanger, F., Carrier, A., Trippanera, D., & Pioli, L. (2022). Geysers, boiling groundwater and tectonics: The 3d subsurface resistive structure of the haukadalur hydrothermal field, iceland [Journal Article]. *Journal of Geophysical Research: Solid Earth*, e2022JB024040.

Mackenzie, G. (1811). *Travels in the island of iceland* [Book]. Edinburgh: Archibald Constable & Co.

Munoz Saez, C., Manga, M., Hurwitz, S., Rudolph, M. L., Namiki, A., & Wang, C. (2015). Dynamics within geyser conduits, and sensitivity to environmental perturbations: insights from a periodic geyser in the el tatio geyser field, atacama desert, chile [Journal Article]. *Journal of Volcanology and Geothermal Research*, *292*, 41-55.

Munoz-Saez, C., Namiki, A., & Manga, M. (2015). Geyser eruption intervals and interactions: examples from el tatio, atacama, chile [Journal Article]. *Journal of geophysical research: Solid Earth*, *120*, 7490-7507.

Namiki, A., Ueno, Y., Hurwitz, S., Manga, M., Munoz-Saez, C., & Murphy, F. (2016). An experimental study of the role of subsurface plumbing on geothermal discharge [Journal Article]. *Geochemistry, Geophysics, Geosystems*, *17*, 3691-3716.

Noguchi, K., Aikawa, K., Lloyd, E., Simpson, B., & van der Werff, P. (1983). Measurement of the orifice temperature of the te horu geyser in whakarewarewa, new zealand [Conference Proceedings]. In *4th int. symp. water-rock interact.* (p. 363-366).

Nogueira, S., Riethmuller, M., Campos, J., & Pinto, A. (2006). Flow patterns in the wake of a taylor bubble rising through vertical columns of stagnant and flowing newtonian liquids: An experimental study [Journal Article]. *Chemical Engineering Science*, *61*, 7199-7212.

Pasvanoglu, S. (1998). Geochemical study of the geysir geothermal field in haukadalur, iceland [Book Section]. In L. Georgsson (Ed.), *United nations university fellows reports 1998* (p. 281-318). UN Univ. Geotherm. Train. Program.

Pinto, A., Coelho Pinheiro, M., & Campos, J. (1998). Coalescence of two gas slugs rising in a co-current flowing liquid in vertical tubes [Journal Article]. *Chemical Engineering Science*, *53*, 2973-2983.

Pioli, A., Palams, M., Behncke, B., De Beni, E., Cantarero, M., & Scollo, S. (2022). Quantifying strombolian activity at etna volcano [Journal Article]. *Geosciences*, *12*, 135.

Pálmason, G. (2002). Iceland's geysir aroused by earthquakes in june 2000 [Journal Article]. *ThE GOSA Transactions*, *7*, 139-147.

Rinehart, J. (1969). Thermal and seismic indications of old faithful geyser's inner workings [Journal Article]. *Journal of geophysical research*, *74*, 566-573.

Rudolph, M. L., & Sohn, R. A. (2017). A model for internal oscillations in geysers, with application to old faithful (yellowstone, usa) [Journal Article]. *Journal of Volcanology and Geothermal Research*, *343*, 17-24.

Rudolph, M. L., Sohn, R. A., & Lev, E. (2018). Fluid oscillations in a laboratory geyser with a bubble trap [Journal Article]. *Journal of Volcanology and Geothermal Research*, *368*, 100-110.

Saemundsson, K. (1979). Outline of the geology of iceland [Journal Article]. *Jökull*, *29*, 7-28.

Schindelin, J., Arganda-Carreras, I., Frise, E., Kaynig, V., Longair, M., Pietzsch, T., . . . Cardona, A. (2012). Fiji: an open-source platform for biological-image analysis [Journal Article]. *Nature Methods*, *9*, 676-682.

Shemer, L., Gulitski, A., & Barnea, D. (2007). On the turbulent structure in the wake of taylor bubbles rising in vertical pipes [Journal Article]. *Physics of Fluids*, *19*, 035108.

Torfason, H. (1985). *The great geysir* (Report). Geysir Conservation Committee.

Torfason, H. (1999). Geology of the geysir area in southern iceland [Conference Proceedings]. In *5th international sympsosium on the geochemistry of the earths surface* (p. 2-5).

Vandemeulebrouck, J., Roux, P., & Cros, E. (2013). The plumbing of old faithful geyser revealed by hydrothermal tremor [Journal Article]. *Geophysical Research Letters*, *40*, 1989-1993.

Vandemeulebrouck, J., Sohn, R. A., Rudolph, M. L., Hurwitz, S., Manga, M., Johnston, M. J., … Murphy, F. (2014). Eruptions at lone star geyser, yellowstone national park, usa: 2. constraints on subsurface dynamics [Journal Article]. *Journal of geophysical research: Solid Earth*, *119*, 8688-8707.

van Hout, R., Gulitski, A., Barnea, D., & Shemer, L. (2002). Experimental investigation of the velocity field induced by a taylor bubble rising in stagnant water [Journal Article]. *International Journal of Multiphase Flow*, *28*, 579-596.

Vergniolle, S., & Jaupart, C. (1986). Separated two-phase flow and basaltic eruptions [Journal Article]. *Journal of Geophysical Research*, *91*(B12), 12,842-12,860.

Viana, F., Pardo, R., Yanez, R., Trallero, J. L., & Joseph, D. D. (2003). Universal correlation for the rise velocity of long gas bubbles in round pipes [Journal Article]. *Journal of Fluid Mechanics*, *494*, 379-398.

Wallis, G. (1969). *One-dimensional two-phase flow* [Book]. New York: McGraw-Hill.

Walter, T., Jousset, P., Allahbakhsi, M., Witt, T., Gudmundsson, M. T., & Hersir, G. (2020). Underwater and drone based photogrammetry reveals structural control at geysir geothermal field in iceland [Journal Article]. *Journal of Volcanology and Geothermal Research*, *391*, 1-9.

White, D. (1967). Some principles of geyser activity, mainly from steambot springs, nevada [Journal Article]. *American Journal of Science*, *265*, 641-684.

White, E., & Beardmore, R. (1962). The velocity of rise of single cylindrical air bubbles through liquids containted in vertical tubes [Journal Article]. *Chemical Engineering Science*, *17*(5), 351-361. doi: https://doi.org/10.1016/0009-2509(62)80036-0